

NULL-FIELD INTEGRAL EQUATION FOR STRESS FIELD AROUND CIRCULAR INCLUSIONS UNDER ANTI-PLANE SHEAR

An-Chien Wu, Wen-Cheng Shen and Jeng-Tzong Chen

*Department of Harbor and River Engineering
National Taiwan Ocean University
Keelung 20224, Taiwan
M93520008@mail.ntou.edu.tw*

ABSTRACT

In this paper, we derive the null-field integral equation for an infinite medium containing circular inclusions with arbitrary radii and positions under remote anti-plane shear. To fully capture the circular geometries, separable expressions of fundamental solutions in the polar coordinate and Fourier series for boundary densities are adopted. By moving the null-field point to the boundary, singular integrals are transformed to series sums after introducing the concept of degenerate kernels. Not only the singularity but also the sense of principle values are novelly avoided. For the calculation of boundary stress, the Hadamard principal value for hypersingularity is not required and can be easily calculated by using series sums. The solution is formulated in a manner of semi-analytical form since error purely attributes to the truncation of Fourier series. The exact solution for a single inclusion is derived. The problem of two inclusions and the problem of one cavity surrounded by two inclusions are revisited to demonstrate the validity of our method. The proposed formulation has been generalized to multiple inclusions and cavities in a straightforward way without any difficulty.

Keywords: anti-plane deformation, null-field integral equation, degenerate kernel, Fourier series, circular inclusion, Laplace problem

1. INTRODUCTION

The problem of stress field around two circular inclusions in an infinite medium under remote shear has been studied by Honein *et al.* [1]. They have introduced the Möbius transformations involving the complex potential to analytically solve the problems. Also the limiting cases of two circular cavities have been examined. For more than two inclusions or cavities, the derivation of an exact solution may have difficulty. Based on the technique of analytical continuity and the method of successive

approximation, Chao and Young [2] have numerically studied the stress distribution on a hole surrounded by two inclusions. To develop a systematic approach for general inclusions or cavities is not trivial. Mogilevskaya and Crouch [3] have solved the problem of an infinite plane containing arbitrary number of circular inclusions based on the complex singular integral equation. In their analysis procedure, the unknown tractions are approximated by using the complex Fourier series. The advantage of their method is that one can tackle a lot of inclusions even inclusions touching one another. However, for calculating an integral over a circular boundary, they did not express the fundamental solution in terms of degenerate kernels using the polar coordinate. Degenerate kernels play an important role not only for mathematical analysis but also for numerical implementation. For example, the spurious eigenvalue [4], fictitious frequency [5] and degenerate scale [6] have been mathematically studied by using degenerate kernels for problems with circular boundaries. Chen *et al.* [7] employed the degenerate kernel and Fourier series to fully capture the geometric property of circular cavities. Besides, they utilized the adaptive observer system and vector decomposition technique to efficiently solve the problem. Three cavities were tested successfully. However, the inclusion was not considered in their paper.

For the circular cavity or inclusion, we use the degenerate kernels in the polar coordinate and Fourier series to best fit the geometry. In this paper, a semi-analytical approach is successfully developed to carry out the solution of the problem under antiplane shear. The mathematical formulation is derived by using degenerate kernels for the fundamental solution and Fourier series expansions for the boundary densities in the null-field integral equation. The continuity and equilibrium constraints on the interface are considered in the multi-domain formulation. By moving the null-field point to the boundary, the singular integral can be easily determined using series sums in our formulation due

to the introduction of degenerate kernels. By substituting the boundary condition, we obtain a linear algebraic system after collocating points on each circular boundary. The unknown coefficients in the algebraic system can be determined. Then, the field potential and stress can be obtained. Furthermore, arbitrary number of circular inclusions can be treated by using the present method without any difficulty. Also, the boundary stress can be easily determined by using series sums instead of employing the sense of Hadamard principal value. A general purpose program for arbitrary number of inclusions with various radii and different positions was developed. The infinite medium with multiple circular holes [7] can be solved as a limiting case of zero shear modulus of inclusions by using the developed program. The exact solution for a single inclusion is derived by using the present formulation. The Honein's problem of two inclusions is revisited to demonstrate the validity of our method. Besides, a hole surrounded by two inclusions solved by Chao and Young [2] is tested to verify the generality for problems including the cavities and inclusions.

2. PROBLEM STATEMENT

The displacement field of the antiplane deformation is defined as:

$$u = v = 0, \quad w = w(x, y), \quad (1)$$

where w is the only nonvanishing component of displacement with respect to the Cartesian coordinate which is a function of x and y . For a linear elastic body, the stress components are

$$\sigma_{13} = \sigma_{31} = \mu \frac{\partial w}{\partial x}, \quad (2)$$

$$\sigma_{23} = \sigma_{32} = \mu \frac{\partial w}{\partial y}, \quad (3)$$

where μ is the shear modulus. The equilibrium equation can be simplified to

$$\frac{\partial \sigma_{31}}{\partial x} + \frac{\partial \sigma_{32}}{\partial y} = 0. \quad (4)$$

Thus, we have

$$\frac{\partial^2 w}{\partial x^2} + \frac{\partial^2 w}{\partial y^2} = \nabla^2 w = 0. \quad (5)$$

Equation (5) indicates that this problem can be modeled by the governing equation of Laplace equation.

We consider an infinite medium subject to N circular inclusions bounded by the B_k contour ($k = 1, 2, \dots, N$) as shown in Fig. 1. The matrix is under remote shear $\sigma_{31}^\infty = 0$, $\sigma_{32}^\infty = \tau$ at infinity or equivalently under the displacement $w^\infty = \frac{\tau y}{\mu}$.

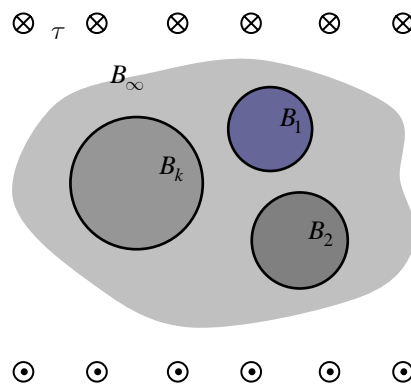


Fig. 1 Infinite antiplane problem with arbitrary circular inclusions

By taking free body on the interface between the matrix and inclusions, we can decompose the problem into two systems as shown in Figs. 2 (a) and 2 (b). In the numerical point of view, this is so-call multi-domain approach. For the problem in Fig. 2 (a), it can be superimposed by two parts as shown in Figs. 2 (c) and 2 (d). Therefore, one exterior problem for the matrix is shown in Fig. 2 (d) and several interior problems for nonoverlapping inclusions are shown in Fig. 2 (b). According to the null-field integral formulation [7], both problems in Figs. 2 (d) and 2 (b) can be solved in a unified manner since they both satisfy the Laplace equation.

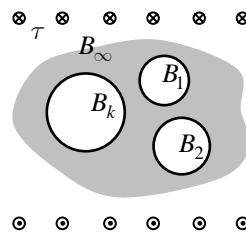


Fig. 2 (a) Infinite medium with holes under uniform shear

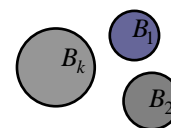


Fig. 2 (b) Interior Laplace problems

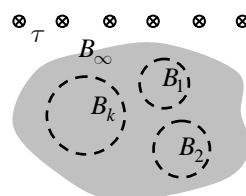


Fig. 2 (c) Infinite medium under uniform shear

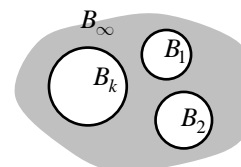


Fig. 2 (d) Exterior Laplace problem

3. A UNIFIED FORMULATION FOR EXTERIOR AND INTERIOR PROBLEMS

3.1 Dual boundary integral equations and dual null-field integral equations

The integral equation for the domain point can be derived from the third Green's identity [8], we have

$$2\pi w(x) = \int_B T(s, x)w(s)dB(s) - \int_B U(s, x)t(s)dB(s), \quad x \in D, \quad (6)$$

$$2\pi \frac{\partial w(x)}{\partial \mathbf{n}_x} = \int_B M(s, x)w(s)dB(s) - \int_B L(s, x)t(s)dB(s), \quad x \in D, \quad (7)$$

where s and x are the source and field points, respectively, B is the boundary, D is the domain of interest, \mathbf{n}_s and \mathbf{n}_x denote the outward normal vector at the source point s and field point x , respectively, and the kernel function $U(s, x) = \ln r$, ($r \equiv |x-s|$), is the fundamental solution which satisfies

$$\nabla^2 U(s, x) = 2\pi\delta(x-s), \quad (8)$$

in which $\delta(x-s)$ denotes the Dirac-delta function. The other kernel functions, $T(s, x)$, $L(s, x)$ and $M(s, x)$, are defined by

$$T(s, x) \equiv \frac{\partial U(s, x)}{\partial \mathbf{n}_s}, \quad L(s, x) \equiv \frac{\partial U(s, x)}{\partial \mathbf{n}_x}, \quad (9)$$

$$M(s, x) \equiv \frac{\partial^2 U(s, x)}{\partial \mathbf{n}_s \partial \mathbf{n}_x},$$

By collocating x outside the domain ($x \in D^c$), we obtain the dual null-field integral equations as shown below

$$0 = \int_B T(s, x)w(s)dB(s) - \int_B U(s, x)t(s)dB(s), \quad x \in D^c, \quad (10)$$

$$0 = \int_B M(s, x)w(s)dB(s) - \int_B L(s, x)t(s)dB(s), \quad x \in D^c, \quad (11)$$

where D^c is the complementary domain. Based on the separable property, the kernel function $U(s, x)$ can be expanded into degenerate form by separating the source points and field points in the polar coordinate [9]:

$$U(s, x) = \begin{cases} U^i(R, \theta; \rho, \phi) = \ln R - \sum_{m=1}^{\infty} \frac{1}{m} \left(\frac{\rho}{R}\right)^m \cos m(\theta - \phi), & R \geq \rho \\ U^e(R, \theta; \rho, \phi) = \ln \rho - \sum_{m=1}^{\infty} \frac{1}{m} \left(\frac{R}{\rho}\right)^m \cos m(\theta - \phi), & \rho > R \end{cases}, \quad (12)$$

where the superscripts "i" and "e" denote the interior ($R > \rho$) and exterior ($\rho > R$) cases, respectively. The origin of the observer system for the degenerate kernel is $(0, 0)$. After taking the normal derivative with respect to Eq. (12), the $T(s, x)$ kernel can be derived as

$$T(s, x) = \begin{cases} T^i(R, \theta; \rho, \phi) = \frac{1}{R} + \sum_{m=1}^{\infty} \left(\frac{\rho^m}{R^{m+1}}\right) \cos m(\theta - \phi), & R > \rho \\ T^e(R, \theta; \rho, \phi) = -\sum_{m=1}^{\infty} \left(\frac{R^{m-1}}{\rho^m}\right) \cos m(\theta - \phi), & \rho > R \end{cases}, \quad (13)$$

and the higher-order kernel functions, $L(s, x)$ and $M(s, x)$, are shown below

$$L(s, x) = \begin{cases} L^i(R, \theta; \rho, \phi) = -\sum_{m=1}^{\infty} \left(\frac{\rho^{m-1}}{R^m}\right) \cos m(\theta - \phi), & R > \rho \\ L^e(R, \theta; \rho, \phi) = \frac{1}{\rho} + \sum_{m=1}^{\infty} \left(\frac{R^m}{\rho^{m+1}}\right) \cos m(\theta - \phi), & \rho > R \end{cases}, \quad (14)$$

$$M(s, x) = \begin{cases} M^i(R, \theta; \rho, \phi) = \sum_{m=1}^{\infty} \left(\frac{m\rho^{m-1}}{R^{m+1}}\right) \cos m(\theta - \phi), & R \geq \rho \\ M^e(R, \theta; \rho, \phi) = \sum_{m=1}^{\infty} \left(\frac{mR^{m-1}}{\rho^{m+1}}\right) \cos m(\theta - \phi), & \rho > R \end{cases}. \quad (15)$$

Since the potential resulted from $T(s, x)$ and $L(s, x)$ kernels are discontinuous cross the boundary, the potentials for $R \rightarrow \rho^+$ and $R \rightarrow \rho^-$ are different. This is the reason why $R = \rho$ is not included in expressional degenerate kernels of $T(s, x)$ and $L(s, x)$ in Eqs. (13) and (14). For circular boundaries, we apply the Fourier series expansions to approximate the potential w and its normal derivative on the boundary

$$w(s_k) = a_0^k + \sum_{n=1}^L (a_n^k \cos n\theta_k + b_n^k \sin n\theta_k), \quad (16)$$

$$s_k \in B_k, \quad k = 1, 2, \dots, N,$$

$$t(s_k) = p_0^k + \sum_{n=1}^L (p_n^k \cos n\theta_k + q_n^k \sin n\theta_k), \quad (17)$$

$$s_k \in B_k, \quad k = 1, 2, \dots, N,$$

where $t(s_k) = \partial w(s_k) / \partial \mathbf{n}_s$, a_n^k , b_n^k , p_n^k and q_n^k ($n = 0, 1, 2, \dots$) are the Fourier coefficients and θ_k is the polar angle. In real computation, only $2L+1$ terms are considered.

3.2 Adaptive observer system

After collocating points in the null-field integral equation of Eq. (10), the boundary integrals through all the circular contours are required. Since the boundary integral equations (BIEs) are frame indifferent, objectivity due to rule, the observer system is adaptively to locate the origin at the center of circle in the boundary integrals. Adaptive observer system is chosen to fully employ the property of degenerate kernels. Figures 3 (a) and 3 (b) show the boundary integration for the circular boundaries in the adaptive observer system. It is worthy noted that the origin of the observer system is located on the center of the corresponding circle under integration to entirely utilize the geometry of circular boundary for the expansion of degenerate kernels and boundary densities. The dummy variable in the circular integration is angle (θ) instead of radial coordinate (R).

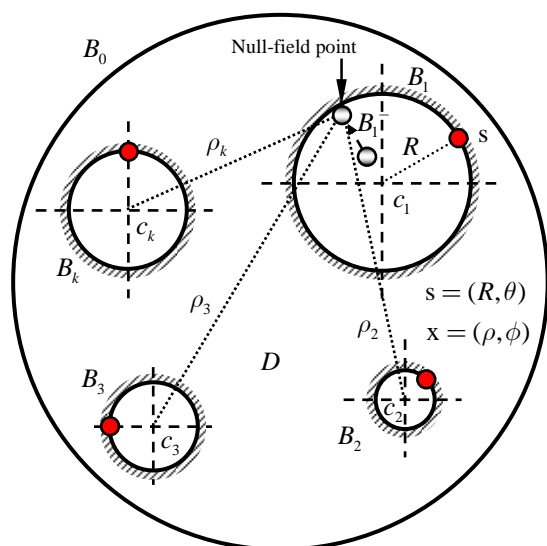


Fig. 3 (a) BIE (null-field point $\rightarrow B_k$)

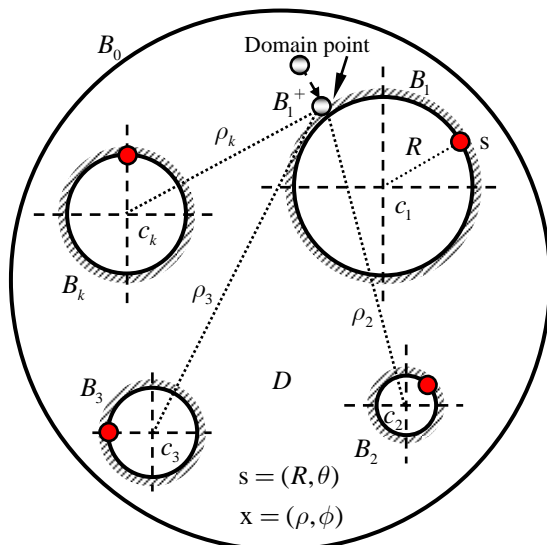


Fig. 3 (b) BIE (domain point $\rightarrow B_k$)

3.3 Linear algebraic system

By moving the null-field point x_j to the j th circular boundary in the limit sense for Eq. (10) in Fig. 3 (a), we have

$$0 = \sum_{k=0}^N \int_{B_k} T(R, \theta; \rho_j, \phi_j) w(R, \theta) R d\theta_k - \sum_{k=0}^N \int_{B_k} U(R, \theta; \rho_j, \phi_j) t(R, \theta) R d\theta_k, \quad (18)$$

$$, x(\rho_j, \phi_j) \in D^c,$$

where N is the number of inner circular inclusion. Note that the kernels U and T are assumed in the degenerate form given by Eqs. (12) and (13), respectively while the boundary densities w and t are expressed in terms of the Fourier series expansion forms given by Eqs. (16) and (17), respectively. Then, the integrals multiplied by separate expansion coefficients in Eq. (10) are non-singular and the limit of the null-field point to the boundary is easily implemented by using appropriate form of degenerate kernels. Thus, the collocation point $x(\rho_j, \phi_j)$ in the discretized Eq.

(10) can be considered on the boundary B_j , too. In contrast to the standard discretized boundary integral equation formulation with nodal unknowns of the physical boundary densities w and t , now the degrees of freedom are given by coefficients employed in the Fourier expansions of these densities. It is found that the compatible relationship of the boundary unknowns is equivalent by moving either the null-field point or the domain point to the boundary in different directions as shown in Figs. 3 (a) and 3 (b). In the B_k integration, we set the origin of the observer system to collocate at the center c_k to fully utilize the degenerate kernels and Fourier series. By collocating the null-field point on the boundary, a linear algebraic system is obtained:

For an exterior problem, we have

$$[\mathbf{U}^M] \{ \mathbf{t}^M - \mathbf{t}^\infty \} = [\mathbf{T}^M] \{ \mathbf{w}^M - \mathbf{w}^\infty \}, \quad (19)$$

For an interior problem, we have

$$[\mathbf{U}^I] \{ \mathbf{t}^I \} = [\mathbf{T}^I] \{ \mathbf{w}^I \}, \quad (20)$$

where the superscripts “ M ” and “ I ” denote the matrix and inclusion, respectively. $[\mathbf{U}^M]$, $[\mathbf{T}^M]$, $[\mathbf{U}^I]$ and $[\mathbf{T}^I]$ are the influence matrices with a dimension of $(N+1)(2L+1)$ by $(N+1)(2L+1)$, $\{ \mathbf{w}^M \}$, $\{ \mathbf{t}^M \}$, $\{ \mathbf{w}^\infty \}$, $\{ \mathbf{t}^\infty \}$, $\{ \mathbf{w}^I \}$ and $\{ \mathbf{t}^I \}$ denote the column vectors of Fourier coefficients with a dimension of $(N+1)(2L+1)$ by 1 in which those can be defined as follows:

$$\begin{aligned}
 [\mathbf{U}^M] &= \begin{bmatrix} \mathbf{U}_{00}^M & \mathbf{U}_{01}^M & \cdots & \mathbf{U}_{0N}^M \\ \mathbf{U}_{10}^M & \mathbf{U}_{11}^M & \cdots & \mathbf{U}_{1N}^M \\ \vdots & \vdots & \ddots & \vdots \\ \mathbf{U}_{N0}^M & \mathbf{U}_{N1}^M & \cdots & \mathbf{U}_{NN}^M \end{bmatrix}, \\
 [\mathbf{T}^M] &= \begin{bmatrix} \mathbf{T}_{00}^M & \mathbf{T}_{01}^M & \cdots & \mathbf{T}_{0N}^M \\ \mathbf{T}_{10}^M & \mathbf{T}_{11}^M & \cdots & \mathbf{T}_{1N}^M \\ \vdots & \vdots & \ddots & \vdots \\ \mathbf{T}_{N0}^M & \mathbf{T}_{N1}^M & \cdots & \mathbf{T}_{NN}^M \end{bmatrix}, \\
 [\mathbf{U}^I] &= \begin{bmatrix} \mathbf{U}_{00}^I & \mathbf{U}_{01}^I & \cdots & \mathbf{U}_{0N}^I \\ \mathbf{U}_{10}^I & \mathbf{U}_{11}^I & \cdots & \mathbf{U}_{1N}^I \\ \vdots & \vdots & \ddots & \vdots \\ \mathbf{U}_{N0}^I & \mathbf{U}_{N1}^I & \cdots & \mathbf{U}_{NN}^I \end{bmatrix}, \\
 [\mathbf{T}^I] &= \begin{bmatrix} \mathbf{T}_{00}^I & \mathbf{T}_{01}^I & \cdots & \mathbf{T}_{0N}^I \\ \mathbf{T}_{10}^I & \mathbf{T}_{11}^I & \cdots & \mathbf{T}_{1N}^I \\ \vdots & \vdots & \ddots & \vdots \\ \mathbf{T}_{N0}^I & \mathbf{T}_{N1}^I & \cdots & \mathbf{T}_{NN}^I \end{bmatrix},
 \end{aligned} \tag{21}$$

$$\begin{aligned}
 \{\mathbf{w}^M\} &= \begin{bmatrix} \mathbf{w}_0^M \\ \mathbf{w}_1^M \\ \mathbf{w}_2^M \\ \vdots \\ \mathbf{w}_N^M \end{bmatrix}, \{\mathbf{t}^M\} = \begin{bmatrix} \mathbf{t}_0^M \\ \mathbf{t}_1^M \\ \mathbf{t}_2^M \\ \vdots \\ \mathbf{t}_N^M \end{bmatrix}, \\
 \{\mathbf{w}^\infty\} &= \begin{bmatrix} \mathbf{w}_0^\infty \\ \mathbf{w}_1^\infty \\ \mathbf{w}_2^\infty \\ \vdots \\ \mathbf{w}_N^\infty \end{bmatrix}, \{\mathbf{t}^\infty\} = \begin{bmatrix} \mathbf{t}_0^\infty \\ \mathbf{t}_1^\infty \\ \mathbf{t}_2^\infty \\ \vdots \\ \mathbf{t}_N^\infty \end{bmatrix}, \\
 \{\mathbf{w}^I\} &= \begin{bmatrix} \mathbf{w}_0^I \\ \mathbf{w}_1^I \\ \mathbf{w}_2^I \\ \vdots \\ \mathbf{w}_N^I \end{bmatrix}, \{\mathbf{t}^I\} = \begin{bmatrix} \mathbf{t}_0^I \\ \mathbf{t}_1^I \\ \mathbf{t}_2^I \\ \vdots \\ \mathbf{t}_N^I \end{bmatrix},
 \end{aligned} \tag{22}$$

where the vectors $\{\mathbf{w}^M\}$, $\{\mathbf{t}^M\}$, $\{\mathbf{w}^\infty\}$, $\{\mathbf{t}^\infty\}$, $\{\mathbf{w}^I\}$ and $\{\mathbf{t}^I\}$ are the Fourier coefficients and the first subscript “ j ” ($j = 0, 1, 2, \dots, N$) in $[\mathbf{U}_{jk}^M]$, $[\mathbf{T}_{jk}^M]$, $[\mathbf{U}_{jk}^I]$ and $[\mathbf{T}_{jk}^I]$ denotes the index of the j th circle where the collocation point is located and the second subscript “ k ” ($k = 0, 1, 2, \dots, N$) denotes the index of the k th circle where boundary data $\{\mathbf{w}^M - \mathbf{w}^\infty\}$, $\{\mathbf{t}^M - \mathbf{t}^\infty\}$, $\{\mathbf{w}^I\}$ or $\{\mathbf{t}^I\}$ are specified, N is the number of circular inclusions in the domain and L indicates the truncated terms of Fourier series.

Two special cases may be solved in a unified manner using the null-field integral formulation:

- (1) One bounded problem of circular domain in Fig. 2 (b) becomes the interior problems.
- (2) The other is unbounded, *i.e.*, the outer boundary B_0 in Fig. 3 (a) is B_∞ . It is the exterior problem.

The direction of contour integration should be taken care, *i.e.*, counterclockwise and clockwise directions are for the interior and exterior problems, respectively. According to the continuity of displacement and equilibrium of traction along the k th interface, we have the two constraints

$$\{\mathbf{w}^M\} = \{\mathbf{w}^I\} \text{ on } B_k, \tag{23}$$

$$[\boldsymbol{\mu}_0]\{\mathbf{t}^M\} = -[\boldsymbol{\mu}_k]\{\mathbf{t}^I\} \text{ on } B_k, \tag{24}$$

where $[\boldsymbol{\mu}_0]$ and $[\boldsymbol{\mu}_k]$ can be defined as follows:

$$\begin{aligned}
 [\boldsymbol{\mu}_0] &= \begin{bmatrix} \mu_0 & 0 & \cdots & 0 \\ 0 & \mu_0 & \cdots & 0 \\ \vdots & \vdots & \ddots & \vdots \\ 0 & 0 & \cdots & \mu_0 \end{bmatrix}, \\
 [\boldsymbol{\mu}_k] &= \begin{bmatrix} \mu_k & 0 & \cdots & 0 \\ 0 & \mu_k & \cdots & 0 \\ \vdots & \vdots & \ddots & \vdots \\ 0 & 0 & \cdots & \mu_k \end{bmatrix},
 \end{aligned} \tag{25}$$

where μ_0 and μ_k denote the shear modulus of the matrix and the k th inclusion. By assembling the matrices in Eqs. (19), (20), (23) and (24), we have

$$\begin{bmatrix} \mathbf{T}^M & \mathbf{U}^M & \mathbf{0} & \mathbf{0} \\ \mathbf{0} & \mathbf{0} & \mathbf{T}^I & \mathbf{U}^I \\ \mathbf{I} & \mathbf{0} & -\mathbf{I} & \mathbf{0} \\ \mathbf{0} & \boldsymbol{\mu}_0 & \mathbf{0} & \boldsymbol{\mu}_k \end{bmatrix} \begin{bmatrix} \mathbf{w}^M \\ \mathbf{t}^M \\ \mathbf{w}^I \\ \mathbf{t}^I \end{bmatrix} = \begin{bmatrix} \mathbf{b} \\ \mathbf{0} \\ \mathbf{0} \\ \mathbf{0} \end{bmatrix}, \tag{26}$$

where $\{\mathbf{b}\}$ and $[\mathbf{I}]$ are the forcing terms due to the remote stress τ and the identity matrix, respectively. After obtaining the unknown Fourier coefficients in Eq. (26), the origin of observer system is set to c_k in the B_k integration as shown in Fig. 3 (b) to obtain the field potential by employing Eq. (6).

3.4 Vector decomposition technique for the potential gradient in hypersingular equation

In order to determine the boundary stress, the tangential derivative should be taken care. Besides, Eq. (7) shows the normal derivative of potential for domain points. For the nonconcentric cases, special treatment for the potential gradient should be taken care as the source point and field point locate on different circular boundaries. As shown in Fig. 4, the

normal direction on the boundary (1, 1') should be superimposed by the radial derivative (3, 3') and angular derivative (4, 4'). We called this treatment "vector decomposition technique". According to the concept of vector decomposition technique, Eqs. (14) and (15) can be modified to

$$L(s, x) = \begin{cases} L^i(R, \theta; \rho, \phi) = \\ -\sum_{m=1}^{\infty} \left(\frac{\rho^{m-1}}{R^m}\right) \cos m(\theta - \phi) \cos(\zeta - \xi) \\ -\sum_{m=1}^{\infty} \left(\frac{\rho^{m-1}}{R^m}\right) \sin m(\theta - \phi) \cos\left(\frac{\pi}{2} - \zeta + \xi\right), R > \rho \\ L^e(R, \theta; \rho, \phi) = \frac{1}{\rho} \\ +\sum_{m=1}^{\infty} \left(\frac{R^m}{\rho^{m+1}}\right) \cos m(\theta - \phi) \cos(\zeta - \xi) \\ -\sum_{m=1}^{\infty} \left(\frac{R^m}{\rho^{m+1}}\right) \sin m(\theta - \phi) \cos\left(\frac{\pi}{2} - \zeta + \xi\right), \rho > R \end{cases}, \quad (27)$$

$$M(s, x) = \begin{cases} M^i(R, \theta; \rho, \phi) = \\ \sum_{m=1}^{\infty} \left(\frac{m\rho^{m-1}}{R^{m+1}}\right) \cos m(\theta - \phi) \cos(\zeta - \xi) \\ -\sum_{m=1}^{\infty} \left(\frac{m\rho^{m-1}}{R^{m+1}}\right) \sin m(\theta - \phi) \cos\left(\frac{\pi}{2} - \zeta + \xi\right), R \geq \rho \\ M^e(R, \theta; \rho, \phi) = \\ \sum_{m=1}^{\infty} \left(\frac{mR^{m-1}}{\rho^{m+1}}\right) \cos m(\theta - \phi) \cos(\zeta - \xi) \\ -\sum_{m=1}^{\infty} \left(\frac{mR^{m-1}}{\rho^{m+1}}\right) \sin m(\theta - \phi) \cos\left(\frac{\pi}{2} - \zeta + \xi\right), \rho > R \end{cases}, \quad (28)$$

where ζ and ξ are shown in Fig. 4. For the special case, the circles with respect to the same origin of observer, the potential gradient is derived free of special treatment since $\zeta = \xi$.

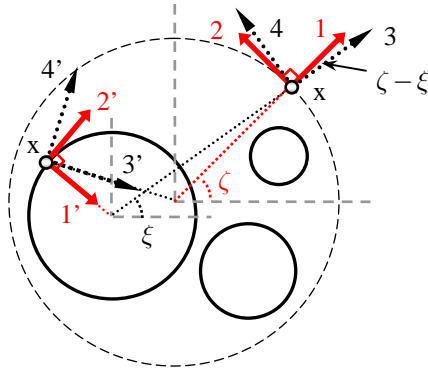


Fig. 4 Vector decomposition

3.5 Stress distribution along the interface

After obtaining all the unknown boundary data w and t for the matrix and inclusions, the boundary stresses in the polar coordinate can be determined by

$$\sigma_{rz} = \sigma_{31} \cos \theta + \sigma_{32} \sin \theta, \quad (29)$$

$$\sigma_{\theta z} = -\sigma_{31} \sin \theta + \sigma_{32} \cos \theta, \quad (30)$$

where σ_{rz} and $\sigma_{\theta z}$ are the normal and tangential stresses. The boundary integral equation for the domain point (including the boundary point) is employed to find the stress by employing appropriate form of degenerate kernels.

4. ILLUSTRATIVE EXAMPLES

First, we derive an analytical solution for a single inclusion. Then, we revisited the two-inclusions problem solved by Honein *et. al.* [1] and the problem of one hole and two inclusions by Chao and Young [2] by using the present method to show the validity of our formulation. All the numerical results are given below by using the twenty terms of Fourier series ($L = 20$).

Case 1: Single inclusion

By using the present formulation, we derived the exact solution of single inclusion perfectly bonded by an infinite medium under uniform shear. The exact solution of the stresses along the circular boundary yields

$$\sigma_{rz}^M = 2\tau \frac{\mu_1}{\mu_0 + \mu_1} \sin \theta, \quad (31)$$

$$\sigma_{\theta z}^M = 2\tau \frac{\mu_0}{\mu_0 + \mu_1} \cos \theta, \quad (32)$$

$$\sigma_{rz}^I = 2\tau \frac{\mu_1}{\mu_0 + \mu_1} \sin \theta, \quad (33)$$

$$\sigma_{\theta z}^I = 2\tau \frac{\mu_1}{\mu_0 + \mu_1} \cos \theta. \quad (34)$$

It is noted that σ_{rz}^M coincides with σ_{rz}^I as required by the traction equilibrium. It is found that stress concentration factor is reduced due to inclusion in comparison with that of cavity ($\mu_1 = 0$) as shown in Eq. (32).

Case 2: Two circular inclusions lie on the y axis

The infinite medium with two elastic inclusions is under uniform shear.

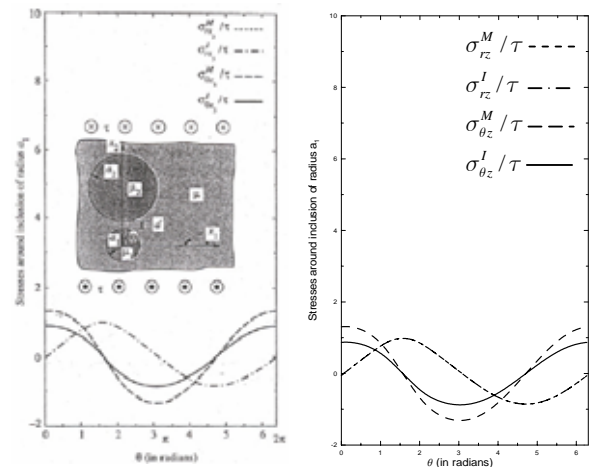


Fig. 5 (a) Honein's data Fig. 5 (b) Present result

The first inclusion centered at the origin of radius a_1 with the shear modulus $\mu_1 = 2\mu_0/3$ and the other inclusion of radius $a_2 = 2a_1$ centered on y

axis at $a_1 + a_2 + d$ ($d = 0.1a_1$) with the shear modulus $\mu_2 = 13\mu_0/7$ are shown in Fig. 5 (a). In order to be compared with the Honein's data obtained by using the Möbius transformation [1], the stresses along the boundary of radius a_1 is shown in Fig. 5 (b). Good agreement is obtained. It satisfies the equilibrium traction along the circular boundary.

Case 3: A circular hole surrounded by two circular inclusions

Figure 6 (a) shows the geometry of one cavity and two inclusions. A circular hole centered at the origin of radius a_1 is surrounded by two circular inclusions ($d/a_1 = 1$) with equal radius $a_2 = 2a_1$, $a_3 = 2a_1$ and equal shear modulus $\mu_2 = \mu_3$. We solved the distribution of the tangential stress along the circular hole influenced by the surrounding inclusions to compare with the Chao and Young's data [2]. The stress distribution along the circular hole affected by the two surrounding inclusions is shown in Figs. 6 (b)-6 (e), when they are arrayed in parallel or perpendicular to the direction of uniform shear. It is noted that the uniform shear at infinity is $\sigma_{31}^\infty = \tau$ and $\sigma_{32}^\infty = 0$. Good agreement is also made.

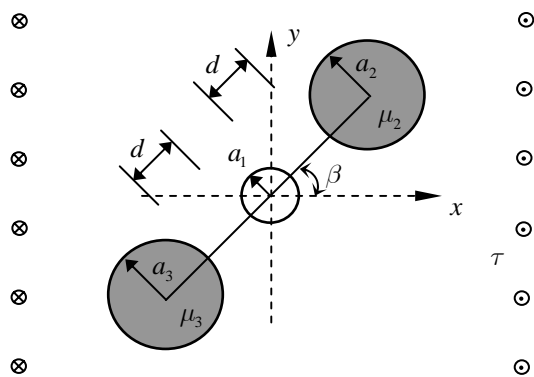


Fig. 6 (a) A circular hole surrounded by two circular inclusions under uniform shear

5. CONCLUSIONS

A semi-analytical formulation for multiple circular inclusions with arbitrary radii and locations using degenerate kernels and Fourier series in an adaptive observer system was developed. The singularity and hypersingularity were avoided after introducing the concept of degenerate kernels. The exact solution for single inclusion was solved by using the present formulation. Two examples investigated by Honein *et al.* and by Chao and Young were revisited, respectively. Good agreements were made after comparing with the previous results. Regardless of the number of inclusions, the proposed method can offer good results. Moreover, our method presented here can be applied to Laplace problems with circular boundaries.

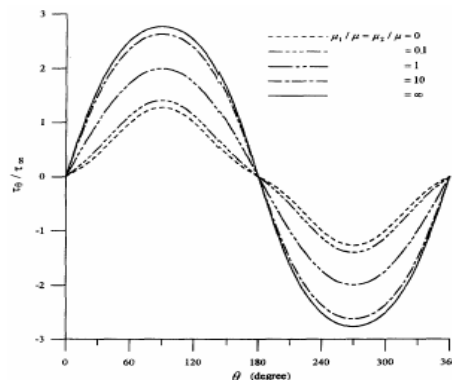


Fig. 6 (b) $\sigma_{\theta z}$ versus θ ($\beta = 0^\circ$) [2]

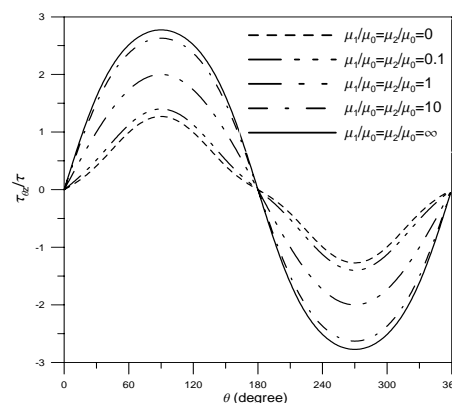


Fig. 6 (c) $\sigma_{\theta z}$ versus θ ($\beta = 0^\circ$) [present result]

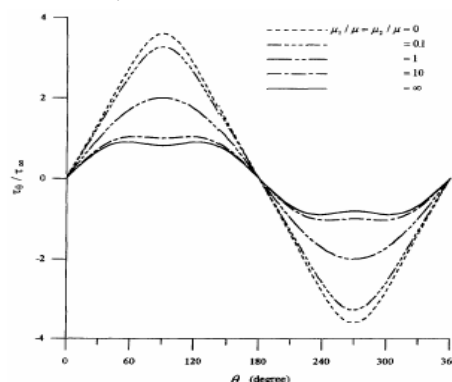


Fig. 6 (d) $\sigma_{\theta z}$ versus θ ($\beta = 90^\circ$) [2]

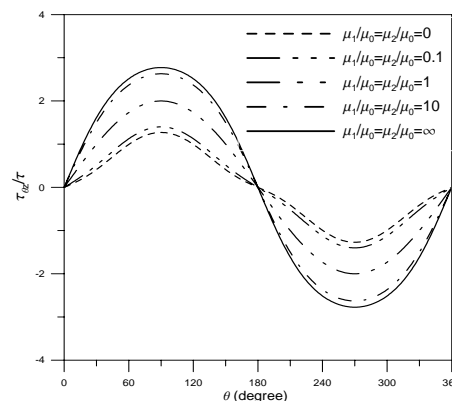


Fig. 6 (e) $\sigma_{\theta z}$ versus θ ($\beta = 90^\circ$) [present result]

REFERENCES

1. E. Honein, T. Honein and G. Herrmann, "On two circular inclusions in harmonic problems," *Quarterly of Applied Mathematics*, Vol. 50, pp. 479-499 (1992).
2. C. K. Chao and C. W. Young, "On the general treatment of multiple inclusions in antiplane elastostatics," *Int. J. Solids Structures*, Vol. 35, pp. 3573-3593 (1998).
3. S. G. Mogilevskaya and S. L. Crouch, "A Galerkin boundary integral method for multiple circular elastic inclusions," *International Journal for Numerical Methods in Engineering*, Vol. 52, pp. 1069-1106 (2001).
4. J. T. Chen, S. R. Kuo and K. H. Chen, "A nonsingular integral formulation for the Helmholtz eigenproblems of a circular domain," *J. Chinese Institute of Engineers*, Vol. 22, No. 6, pp. 729-739 (1999).
5. J. T. Chen and S. R. Kuo, "On fictitious frequencies using circulants for radiation problems of a cylinder," *Mechanics Research Communications*, Vol. 27, No. 1, pp. 49-58 (2000).
6. J. T. Chen, S. R. Kuo and J. H. Lin, "Analytical study and numerical experiments for degenerate scale problems in the boundary element method for two-dimensional elasticity," *Int. J. Numer. Meth. Engng.*, Vol. 54, No. 12, pp. 1669-1681 (2002).
7. J. T. Chen, W. C. Shen and A. C. Wu, "Null-field integral equations for stress field around circular holes under antiplane shear," *Engineering Analysis with Boundary Elements*, Accepted (2005).
8. J. T. Chen and H-K Hong, "Review of dual boundary element methods with emphasis on hypersingular integrals and divergent series," *ASME Applied Mechanics Reviews*, Vol. 52, pp. 17-33 (1999).
9. J. T. Chen and Y. P. Chiu, "On the pseudo-differential operators in the dual boundary integral equations using degenerate kernels and circulants," *Engineering Analysis with Boundary Elements*, Vol. 26, pp. 41-53 (2002).
10. W. C. Shen, "Null-field approach for Laplace problems with circular boundaries using degenerate kernels," Master Thesis, *Department of Harbor and River Engineering, National Taiwan Ocean University*, Keelung, Taiwan (2005).

零場積分方程求解含圓形置入物受反平面剪力之應力場

吳安傑 沈文成 陳正宗

國立台灣海洋大學 河海工程學系

摘要

本文係使用零場積分方程式求解基材含任意大小、位置之圓形置入物或孔洞，受反平面剪力作用下之應力場。將基本解以極座標展開成退化核(分離核)的形式，而以傅立葉級數來完整描述邊界物理量。藉由引入退化核的觀念，將零場點推向邊界時，奇異積分會被轉換成級數和的形式。因此無需面對奇異積分，且在計算邊界應力時，不需處理 Hadamard 主值問題，而可輕易地由級數和的形式求得。由於誤差僅來自於擷取有限項的傅立葉級數，故本方法可視為“半解析法”。由於本方法可輕易導得單一置入物的解析解，因此我們分別求解含兩個圓形置入物與兩個圓形置入物圍繞單一圓洞的問題來突顯本方法的一般性。最後，我們提出一套系統性的方法來求解含多圓洞與置入物的反平面問題。

關鍵字：反平面、零場積分方程式、退化核(分離核)、傅立葉級數、圓形置入物、拉普拉斯方程式